Journal of Structural Geology 155 (2022) 104512

Contents lists available at ScienceDirect

Journal of Structural Geology

journal homepage: www.elsevier.com/locate/jsg

Using the Schmidt hammer on folds: An example from the Cantabrian Zone (NW Iberian Peninsula)

J. Poblet [a,*], M. Bulnes [a], H. Uzkeda [b], M. Magán [a]

[a] Departamento de Geología, Universidad de Oviedo, C/Jesús Arias de Velasco s/n, 33005, Oviedo, Spain, EU
[b] Terractiva, Rda. Sant Pere 52, 08010, Barcelona, Spain, EU

ARTICLE INFO

Keywords:
Schmidt hammer rebound
Rock resistance
Fold
Cantabrian zone

ABSTRACT

The Schmidt hammer, widely used in Engineering Geology, has also been used in Structural Geology as a tool to quantify the mechanical properties of rocks affected by different structures and the damage caused to rocks by fracturing. However, how the impact resistance of rocks (rebound) varies in layers located in different positions of a fold has never been tested. Here, the Schmidt hammer is used to quantify this parameter in a syncline involving a Carboniferous carbonate sequence located in the Cantabrian Zone, the foreland fold-and-thrust belt of the Variscan orogen in western Iberia. The variations in the Schmidt-hammer rebound value along a folded layer are consistent with other indicators such as variations of dip and thickness. These findings have also implications on obtaining representative rebound values of stratigraphic units, and on deriving parameters such as the uniaxial compressive strength and the Young modulus from the Schmidt-hammer rebound values applied to folded regions.

1. Introduction

A Schmidt hammer is a non-destructive tool that measures the resistance of materials to impact penetration by a plunger tip as a rebound value. The lower the rebound value the lower the resistance and vice versa. Notable contributions have been made in the application of the Schmidt hammer to Structural Geology (Katz et al., 2003; Greco and Sorriso-Valvo, 2005; Shackleton et al., 2005; Morris et al., 2009; Savage et al., 2010; Smart et al., 2010, 2012, 2014; Zahm et al., 2010; Steer et al., 2011; Ferrill et al., 2011, 2012a, b, 2014, 2016; McGinnis et al., 2017; Torabi et al., 2018; Tye and Stahl, 2018; Stahl and Tye, 2020) focused on characterizing the mechanical properties of successions of rocks affected by fractures and folds, and determining how the rebound values vary in faulted and jointed rocks. However, as far as we know, this hammer has never been used to quantify rebound values in a particular bed whose dip changes, i.e., a folded layer. Thus, the main goal of this study is to check whether the rebound values of the Schmidt hammer in specific layers located in the hinge and in the limbs of a particular fold are constant or they vary, and if they are variable, whether the rebound values are or are not consistent with other folding indicators.

The Cantabrian Zone is the foreland fold-and-thrust belt of the Variscan orogen located in the northwest portion of the Iberian Peninsula (Fig. 1). It includes abundant folds of different types (related and unrelated to faults), of different scales (millimetre to kilometre-scale), with different shapes (from rounded to chevron to box), with different interlimb angles (from gentle to tight), and affecting different lithological types (siliciclastic rocks, carbonates, coal, etc.) (e.g., Julivert, 1971, 1979, 1981, 1983; Savage, 1979, 1981; Pérez-Estaún et al., 1988; Pérez-Estaún and Bastida, 1990; Aller et al., 2004). Therefore, it is an excellent natural laboratory to carry out this type of study.

A metre-scale syncline, developed in Carboniferous carbonate rocks, has been chosen to perform this experiment because of its excellent outcrop quality in a slope of a local road in the province of León, Spain (Fig. 2). This syncline is accessible from the road by a standing person or using a foldable ladder, the folded rocks do not show evidence of intense weathering, the layers can be followed from one fold limb to the other through the fold hinge, the rocks exhibit faces that allow measuring dips, stratigraphic thicknesses and Schmidt hammer rebounds in different directions, and the fold shape varies up section.

2. Methodology

An N-type Schmidt hammer manufactured by the company Proceq

* Corresponding author.
E-mail addresses: jpoblet@geol.uniovi.es (J. Poblet), maite@geol.uniovi.es (M. Bulnes), hodei@terractiva.net (H. Uzkeda), maganmarta@uniovi.es (M. Magán).

https://doi.org/10.1016/j.jsg.2022.104512
Received 30 September 2021; Received in revised form 22 December 2021; Accepted 2 January 2022
Available online 6 January 2022

has been used, with a normalized impact energy of 2.207 Nm and with a correction factor of 1. According to the Proceq (2016) manual instructions, this device does not need corrections related to the gravity force. The collected data have been treated using the Standard Test Method for Determination of Rock Hardness by Rebound Hammer Method ASTM D 5873 (ASTM, 2001). This method requires 10 impacts in each location, a mean is calculated, individual rebound values that diverge more than 7 from the calculated mean are discarded, and a new mean is calculated using the remaining values. In order to avoid wrong measurements, we have followed the rules recommended in the Proceq (2016) manual and in Aydin and Basu (2005) to collect the data, i.e., impacts as perpendicular as possible to the rock faces to be measured and in close but different places, avoiding rock faces with alteration patina and/or moss/lichens, also avoiding rough surfaces, and under similar moisture conditions. Although the initial strategy of measurement positioning was a regular measurement grid, only some localities accomplished the sampling rules, and this is why a random sampling has been be adopted (Fig. 1 in supplementary material). We have tried to uniformly distribute the Schmidt hammer measurements in eight layers and throughout the fold limbs and hinges. The minimum distance between measurements within the same layer is 30 cm, while the maximum is approximately 1.5 m. The minimum distance between measurements of the same structural position (southwest limb, hinges, northeast limb) made in different layers is 11 cm, while the maximum is approximately 45 cm. 55 valid Schmidt hammer measurements parallel to the syncline axis have been used (Table 1 in supplementary material). Additionally, some measurements parallel to bedding and perpendicular to the syncline axis, and perpendicular to bedding when possible have been collected. We have discarded those localities in which the number of valid impacts has been much less than 10 and the standard deviation has been very high; in these cases the measurements have been repeated in a nearby locality. Nevertheless, we have accepted localities with low impact numbers and high standard deviations when all the measurements in neighboring localities have these same characteristics, but we considered necessary to obtain a measurement to keep the distance between localities relatively small, and therefore, construct rebound isocontours based on sufficient values. We have not identified any specific distribution pattern of the standard deviation in terms of structural position of the measurements or in terms of the layers. The values obtained in the different localities have been analysed independently for each layer.

In addition, a virtual outcrop model of the syncline based on a point-cloud has been constructed using the photogrammetric procedure known as "structure from motion" (Wu, 2013) and the software Pix4DMapper. This strategy, based on processing a large number of high-dynamic-range photographs of the outcrop taken with a conventional photographic camera mounted on a tripod, is described in detail in Martín et al. (2013, 2019) and Uzkeda et al. (2018). The virtual outcrop model has been scaled multiplying the coordinates of the raw point cloud by a factor. This factor has been calculated comparing the length of several segments measured in the field in different directions and their random length on the raw point cloud. A similar approach has been used to determine the correct orientation of the point cloud; thus, the original point cloud has been rotated using the orientation of several planes measured in the field as a reference. Moreover, a texturized triangular mesh of the outcrop has been constructed using the software Pix4DMapper for the purposes of description and visualization of the structure (Fig. 2). Nevertheless, the geological interpretation has been carried out on the point cloud to avoid problems derived from the interpolation necessary to create the mesh. A distortion-free geological profile, perpendicular to the syncline axis, has been constructed by projecting the geological interpretation of the virtual outcrop model onto an appropriate plane using the syncline axis measured in the field (Fig. 3) as projection direction. Both the geological interpretation and the cross-section construction have been carried out using the software Move. Dips, stratigraphic thicknesses and Schmidt hammer measurements taken in the field have been located onto the geological profile and their values have been interpolated using the free software QGis (QGis.org Association, 2021) (Fig. 4).

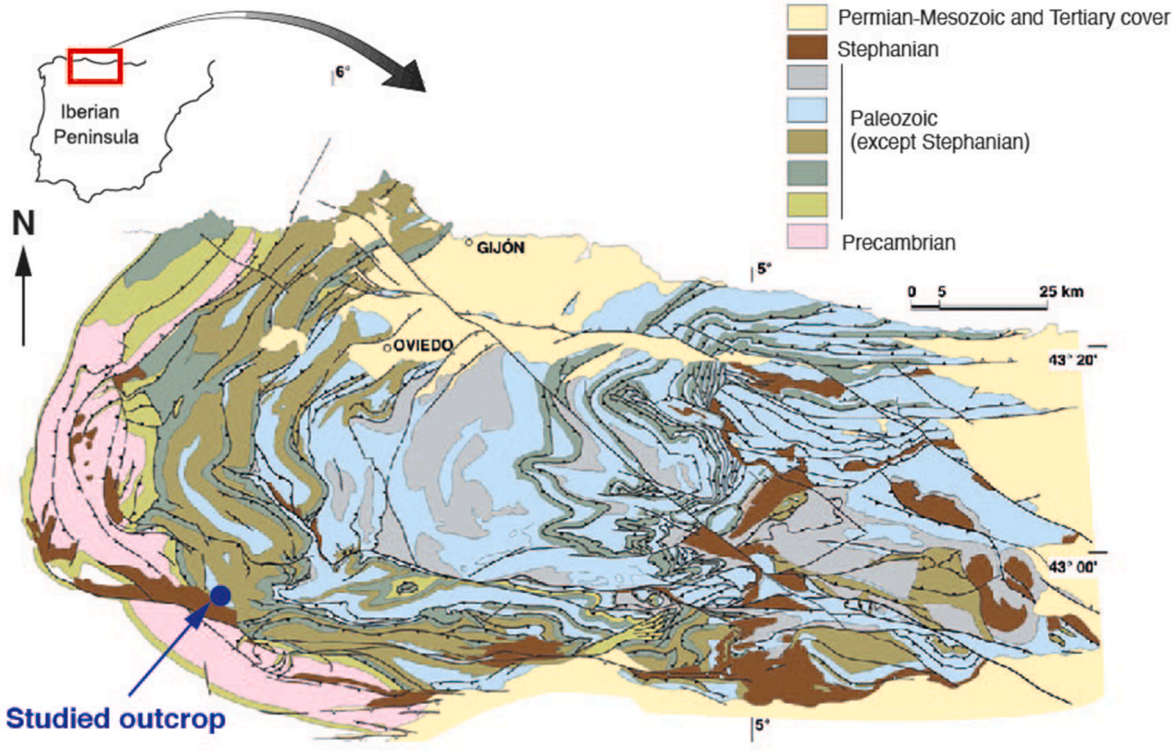

Fig. 1. Simplified structural sketch of the Cantabrian Zone with location of the studied outcrop.

3. Geological setting

The selected outcrop is located in the southwestern part of the Cantabrian Zone, which is the foreland fold-and-thrust belt of the West-Iberia Variscan Orogen (Lotze, 1945; Julivert et al., 1972) (Fig. 1). The Cantabrian Zone involves a Palaeozoic stratigraphic succession from Cambrian to Carboniferous, made up of both siliciclastic (slates, sandstones and microconglomerates) and carbonate (marls, limestones and dolomites) sedimentary rocks with sporadic coal beds and volcanic rocks. The Cantabrian Zone developed under diagenetic conditions, although some localities reached very low or low-grade metamorphism. It is a typical thin-skinned belt, constituted by different types of thrust systems and folds, where tectonic foliations are lacking except for small areas (e.g., Julivert, 1971, 1979, 1981, 1983; Savage, 1979, 1981; Pérez-Estaún et al., 1988; Pérez-Estaún and Bastida, 1990; Aller et al., 2004; Alosno et al., 2009). In cross-sectional view, the Cantabrian Zone exhibits a wedge shape thinning eastwards, i.e., towards the foreland. In map view, it displays a curved trend around an approximately E–W axial surface with the inner core to the east, known as Ibero-Armorican or Asturian Arc (Fig. 1). The studied outcrop is located in the south branch of this orocline.

From the structural point of view, the studied syncline (Fig. 2) is a second-order fold developed in the southwest limb of a tight, NW-SE syncline of kilometre-scale, whose axial surface is subvertical and is called Vega de Los Viejos Syncline (geological map and section II-II' in Navarro Vázquez and Rodríguez Fernández, 1982, Figs. 3 and 4 in Bastida et al., 1984; Alonso et al., 1989). This large syncline, developed during the Variscan orogenesis of Carboniferous age, involves an Ordovician-Carboniferous succession unconformably covered by Stephanian (Uppermost Carboniferous) deposits on the southwestern limb of the syncline.

4. Stratigraphy

The rocks involved in the studied syncline are dark grey to black micritic limestones, with some marly limestones intercalated (Fig. 2). The layer thickness ranges from laminated beds to decimetre-thickness beds, and bedding surfaces are usually smooth and well developed. These rocks often include very striking, small veins filled in with white calcite perpendicular to bedding but also following other directions. All these carbonate rocks belong to the upper part of the Barcaliente Fm. (Wagner et al., 1971), a Carboniferous unit which reaches a few hundred metres thickness in the study area (Navarro Vázquez and Rodríguez Fernández, 1982; Bastida et al., 1984).

5. Syncline structure

The studied syncline (Fig. 2), flanked by two anticlines, consists of long, approximately straight limbs and narrow hinges compared to the limbs, and has a chevron-shaped inner core and a box-fold outer core (Figs. 2 and 4). It is an asymmetrical fold, whose southwest limb reaches more than 3.5 m length and dips approximately 40° to the NE, while its northeast limb reaches a length less than 3 m and dips from 70 to almost 90° to the SW. The fold trough developed in the outer core of the syncline is almost 1.5 m long and dips less than 5° to the SW. The interlimb angle measured in the chevron-folded inner core is around 70°, and therefore, it is a close fold. This syncline is an approximately cylindrical fold (Fig. 3), whose axis dips from 10 to 20° to the NW, and whose northeast axial surface strikes NW-SE and dips 50° to the NE, while its southwest axial surface also strikes NW-SE but dips approximately 70° to the SW.

The studied syncline is not a parallel fold. The maximum thickness across the fold occurs in the syncline hinges, in particular in the northeast hinge (Fig. 4a). The maximum thickening measured reaches 75%, i.e., a layer in one of the syncline hinges is 175% thicker than the same layer in one of the syncline limbs. The thickening takes place in an apparently ductile manner, by means of small-scale second-order folds, and/or by means of small-scale thrusts responsible for layer duplication (Fig. 5). The thrust surfaces strike NW-SE and their slickensides, approximately perpendicular to the syncline axis, indicate dip-slip motion (Fig. 3). These thickness variations roughly coincide with the regions in which the greatest variations in dip of the layers occur (Fig. 4b).

Fig. 2. Image of a texturized triangular mesh showing the studied syncline in the central part of the picture. The eight beds analysed here are located in the central-lower part of the syncline.

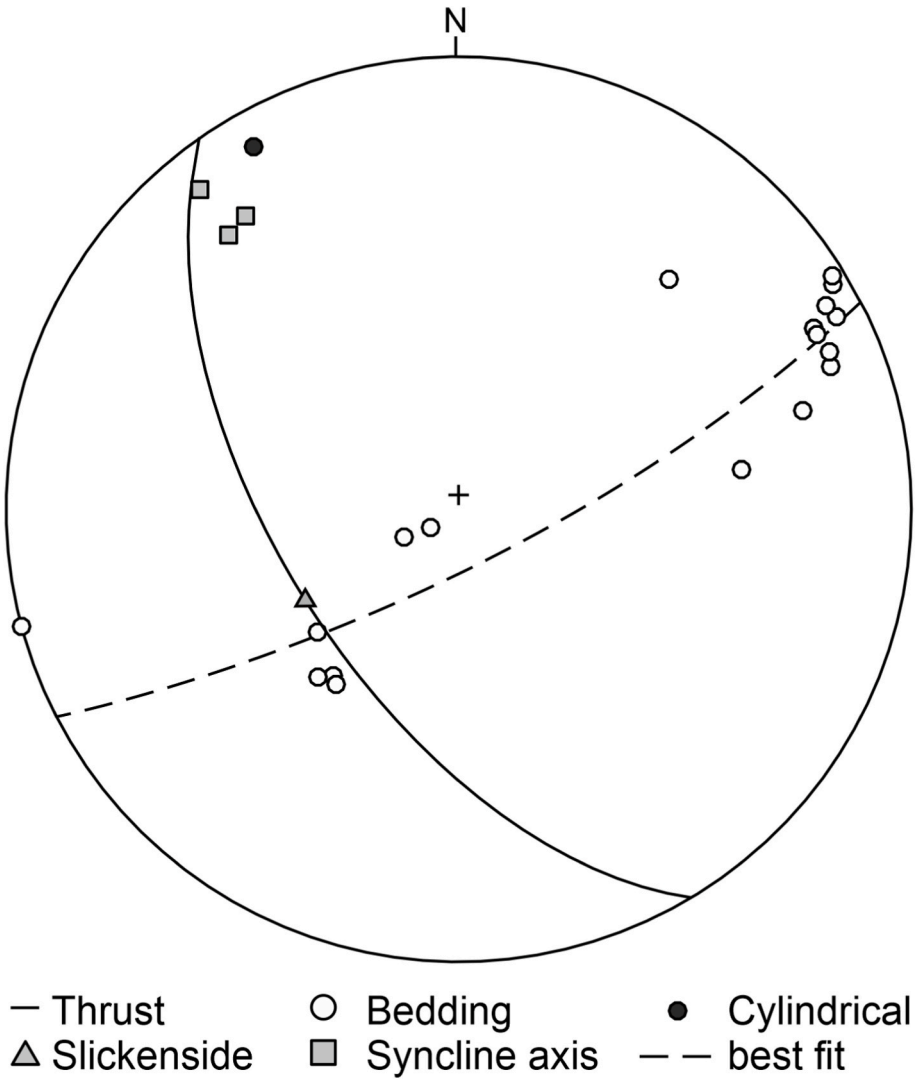

Fig. 3. Equal area projection in the lower hemisphere, constructed using an in-house script written in Octave computational language by H. Uzkeda, showing the orientation of bedding, fold axes, a thrust and its kinematic indicators, and the best-fit cylindrical plane for the bedding data. Although the syncline may be slightly conical, a cylindrical best fit is good enough for the purpose of the 2D study carried out here.

All the observations above point out that the hinges are more strained than the limbs, similarly to other structures developed in Carboniferous limestones and marls in nearby locations analysed using cross-section restoration techniques including strain markers (Masini et al., 2010a, b; Bulnes et al., 2019).

6. Schmidt-Hammer rebound values

The rebound values obtained range from almost 20 to almost 70. In outline, the Schmidt-hammer rebound values for each single layer are lower in the hinges than in the fold limbs (Fig. 4c). The maximum percentage of rebound variation obtained within a single layer is almost 65%, so that the less resistant part of a layer located in one of the syncline hinges has a rebound value which is 35% of the value for that same layer in one of the syncline limbs. Thus, the Schmidt hammer data collected are consistent with the observations made from thickness, small-scale structures and dip changes across the syncline (Fig. 4a and b, 5). The regions most thickened through several types of second-order structures and with greater dip variations, i.e., the syncline hinges, exhibit lower Schmidt-hammer rebound values, and vice versa for the fold limbs (Fig. 4a, b and c). Schmidt-hammer rebound values are related to impact rock resistance, that, apart from rock rheology, depend on the density of fractures (e.g., Katz et al., 2003; Greco and Sorriso-Valvo, 2005). On the contrary, changes in thickness and dip of the layers across a fold are mainly related to strain. The observations above point out that, at least for the studied syncline, the higher the strain suffered by the rocks the less the rock resistance, and therefore, the higher the number of fractures. As mentioned above, hinge zones where the thickening have taken place through second-order folds and faults, but also in an apparent ductile manner, exhibit low rebound values. This suggests that, although the thickening appears to be ductile in some localities, it may be due to microfractures not directly visible in the outcrop. However, this should be confirmed with microscopical observations of thin sections that are beyond the scope of this study.

It is well known that the dip of the layers involved in a fold is not an indicator of the strain suffered by them, since horizontal layers may have been more strained than inclined layers. This depends on fold kinematics (e.g., Salvini and Storti, 2001; Poblet, 2020). The studied syncline is a good example reflected in the Schmidt-hammer rebound values. Thus, moderately to steeply dipping beds in the limbs have higher rebound values than sub-horizontal beds in the syncline crest (Fig. 4c). The distribution of the low rebound values along the entire syncline trough might be diagnostic of fold amplification through a hinge migration mechanism (Suppe, 1983) or a combination of hinge

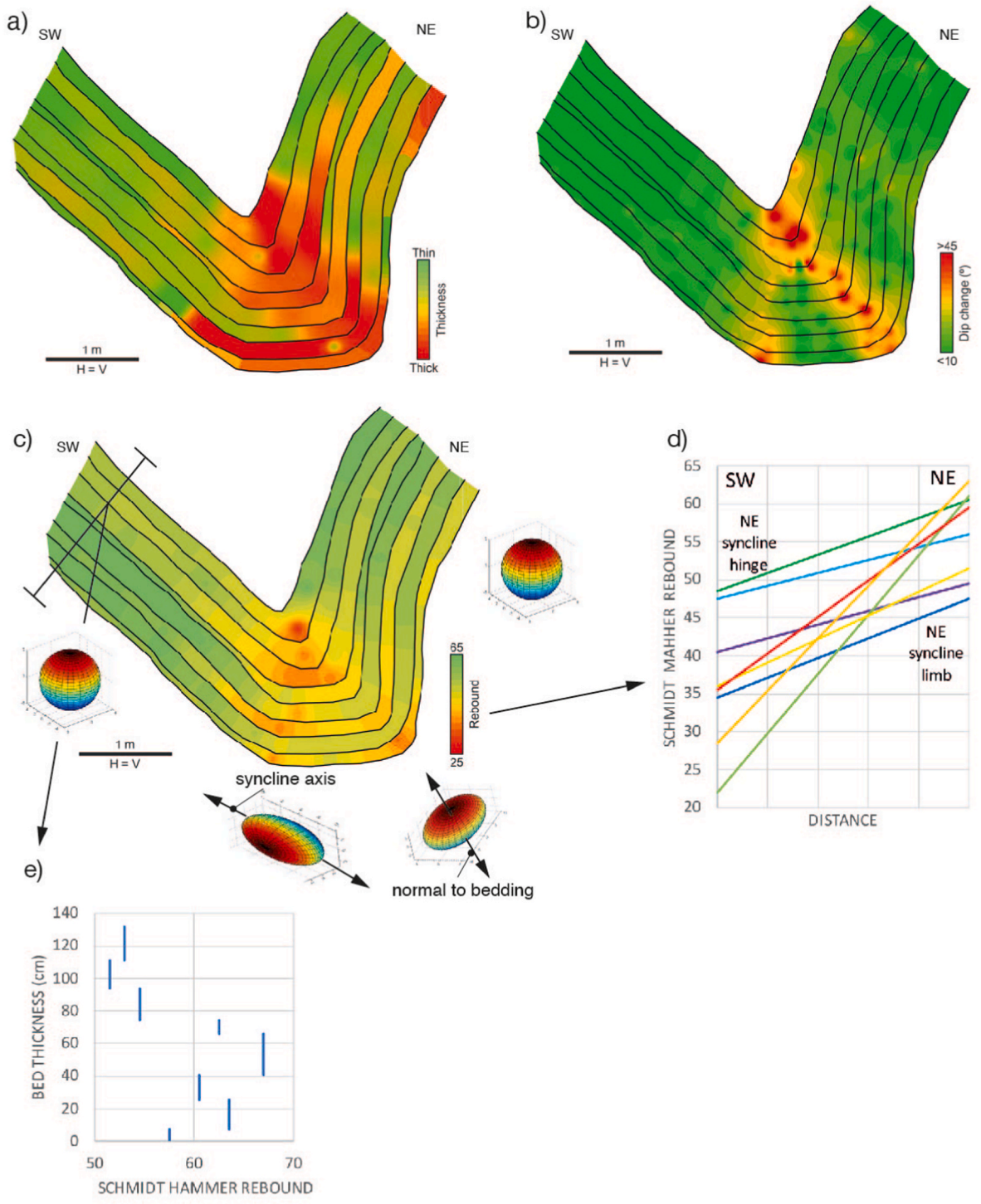

Fig. 4. Geological profiles across the studied syncline, derived from the geological interpretation of the virtual outcrop model, including a) isopachs constructed using 67 thickness measurements, b) contours of equal dip variation constructed using 21 dip measurements, and c) contours of equal Schmidt hammer rebound constructed using data from 55 localities. To construct the dip change isocontours we calculated the dip difference at each bend/dip change along the bedding surfaces. 3D spheres and ellipsoids of Schmidt-hammer rebound values using measurements parallel to the syncline axis, parallel to bedding and perpendicular to the syncline axis, and perpendicular to bedding are shown in figure c). d) Schmidt-hammer rebound values for the eight beds shown in figures a), b) and c) (illustrated with different colours) in the northeast syncline limb and in the northeast syncline hinge. e) Graph showing the rebound values for the eight beds depicted in figures a), b) and c) in the southwest syncline limb. Beds have been analysed independently in figures a), c), d) and e). (For interpretation of the references to colour in this figure legend, the reader is referred to the Web version of this article.)

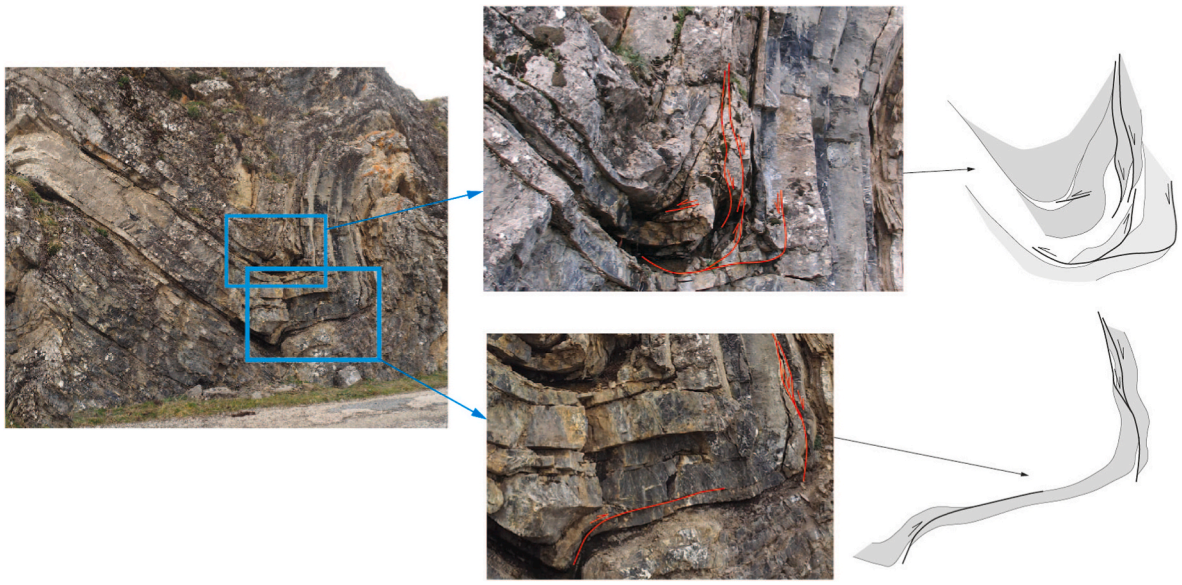

Fig. 5. Photograph of the studied syncline showing the main second-order structures related to fold amplification (folded thrusts) that caused hinge thickening.

migration plus limb rotation (Beutner and Diegel, 1985), since in the case of pure limb rotation, the low rebound values would be concentrated around the syncline hinges (Salvini and Storti, 2001; Poblet, 2020).

In all the layers the Schmidt-hammer rebound value decreases progressively in a similar way from the syncline limbs towards the hinge (Fig. 4d). Thus, when in one syncline limb a layer has a rebound value greater than that of another layer, in the hinge zone, this relationship between the rebound values of the two layers is still maintained despite the fact that both layers have lower rebound values than the ones they had in the limb. However, occasionally that relationship can be reversed at the hinge, so that the layer with the highest rebound value in the syncline limb is the one with the lowest rebound value in the hinge. For instance, Fig. 4d shows how, in the northeast limb, the rebound values of the layers represented with yellow, red and green colours are higher than the rebound values of the layers represented in light blue and purple. However, in the northeast hinge zone, the layers depicted in yellow, red, and green have lower rebound values than the layers depicted in light blue and purple. This suggests that the mechanical properties of rocks subjected to folding can change to such an extent that the supposedly "most resistant beds" in the least folded structural positions (i.e., fold limbs), may become the "least resistant beds" in the most folded structural positions (i.e., fold hinges).

If we construct hypothetical stratigraphic columns to show the rebound values of different layers in different portions of the syncline, i.e., on the southwest limb, on each fold hinge and on the northeast limb, we conclude the following. Layers with very similar lithologies and thicknesses, located in the same structural position with respect to the syncline and under the same pressure and temperature conditions, exhibit different rebound values (Fig. 4e). Thus, to understand the variation in the rebound values across a fold we must stick to the data taken in each of the layers independently and we must not compare data obtained from different layers.

A few Schmidt hammer measurements in different space directions have also been taken. In both syncline limbs, the Schmidt-hammer rebounds obtained in different directions are very similar resulting in a three-dimensional rock resistance almost spherical, although the magnitude perpendicular to bedding is slightly greater than the other two (Fig. 4c). In the southwest syncline hinge, the rebound obtained in several directions is similar except for the rebound parallel to the fold axis which is greater. Thus, the three-dimensional rock resistance in this hinge forms a prolate-type ellipsoid, being the fold axis the direction of greatest rock resistance (Fig. 4c). This result is in accordance with the dip data; thus, since the syncline is approximately cylindrical (Fig. 3), the syncline axis direction is the minimum curvature direction and the less fractured one, and therefore, the most resistant. However, in the northeast syncline hinge, the rebound values obtained in different directions are similar except for the rebound value perpendicular to bedding which is lower. Thus, the three-dimensional rock resistance in this hinge is an oblate-type ellipsoid where the direction perpendicular to bedding is the least resistant (Fig. 4c). The difference between the prolate ellipsoid in the southwest synclinal hinge and the oblate ellipsoid in the northeast synclinal hinge could be explained as a function of the interlimb angle in both hinges. The interlimb angle in the southwest hinge is almost 140°, and therefore, it corresponds to a gentle fold, while the interlimb angle in the northeast hinge is almost 100°, and therefore, it is an open fold. Thus, the southwestern hinge is less tight than the northwestern one, which is more curved and thickened (Fig. 4a and b). In our opinion, the syncline cylindricity criterion prevails in the relatively open southwest hinge, and therefore, the rock resistance measured in the direction parallel to the fold axis is the greatest. However, the rocks have exceeded a threshold in the tighter northeast hinge, so that folding has caused a notable decrease in their resistance perpendicular to bedding.

7. Conclusions

The use of the Schmidt hammer in folded areas, following the strategy outlined here, provides quantitative values approximately consistent with other folding indicators such as dip and thickness variations both in 2 and 3 dimensions. Thus, the Schmidt hammer rebound may be an additional parameter for fold characterization.

Estimating Schmidt-hammer rebound values in some beds and assuming they are representative of the whole stratigraphic unit is not recommended no matter whether the unit is made up of a single lithology, because different rebound values have been obtained for layers whose lithology and thickness are almost identical and have been subjected to the same environmental conditions. Thus, each layer must be treated independently. In case we need to estimate an average rebound value of a stratigraphic unit, we recommend obtaining a value for each layer and averaging it taking into account the percentage each layer represents within the stratigraphic unit estimated according to its thickness.

Great caution must be taken when collecting Schmidt-hammer

rebound values of rocks in folded regions, specifically when they are used to estimate parameters such as the uniaxial compressive strength and the Young modulus, something that has been done since the 1960s (e.g., Deere and Miller, 1966). Thus, even for a single layer with a uniform lithological composition, the rebound values may be different depending on its structural position within a fold. The fact that the rebound values are measured in horizontal layers does not a guarantee that they are representative. A structural study is necessary.

Author statement

Josep Poblet: Conceptualization, Methodology, Validation, Investigation, Resources, Writing - original draft, Writing – review & editing, Supervision, Project administration, Funding acquisition.

Mayte Bulnes: Methodology, Validation, Investigation, Resources, Writing – review & editing, Visualization, Supervision, Project administration, Funding acquisition.

Hodei Uzkeda: Methodology, Software, Resources, Writing – review & editing, Visualization.

Marta Magán: Methodology, Resources, Writing – review & editing, Visualization.

Declaration of competing interest

The authors declare that they have no known competing financial interests or personal relationships that could have appeared to influence the work reported in this paper.

Acknowledgments

This study has been supported by research projects CN-16-014, CN-16-015 and CN-16-016 funded by the oil company Repsol. We thank Petroleum Exploration Experts for permission to use the software Move (Contract reference Agr_ULA_UniOviedo_18_11_01). The main editor and the editors of this special issue: Ian Alsop, Catalina Luneburg, Djordje Grujic, Stefano Mazzoli and Hermann Lebit, as well as two reviewers, are gratefully acknowledged. We hope this study is worthy of contributing to the tribute to John G. Ramsay, probably the best structural geologist of all times.

Appendix A. Supplementary data

Supplementary data to this article can be found online at https://doi.org/10.1016/j.jsg.2022.104512.

References

Aydin, A., Basu, A., 2005. The Schmidt hammer in rock material characterization. Eng. Geol. 81 (1), 1–14.
ASTM, 2001. Standard Test Method for Determination of Rock Hardness by Rebound Hammer Method. ASTM Stand, 04.09 (D 5873-00).
Aller, J., Álvarez-Marrón, J., Bastida, F., Bulnes, M., Heredia, N., Marcos, A., Pérez-Estaún, A., Pulgar, J.A., Rodríguez-Fernández, R., 2004. Estructura, deformación y metamorfismo (Zona Cantábrica). In: Vera, J.A. (Ed.), Geología de España. Sociedad Geológica de España-Instituto Geológico y Minero de España, Madrid, pp. 42–49.
Alonso, J.L., Álvarez-Marrón, J., Pulgar, J.A., 1989. Síntesis cartográfica de la parte sudoccidental de la Zona Cantábrica. Trab. Geol. 18, 145–155.
Alosno, J.L., Marcos, A., Suárez, A., 2009. Paleogeographic inversion resulting from large out of sequence breaching thrusts: the León fault (Cantabrian zone, NW Iberia). A new picture of the external Variscan thrust belt in the Ibero-Armorican arc. Geol. Acta 7 (4), 451–473.
Bastida, F., Marcos, A., Pérez-Estaún, A., Pulgar, J.A., 1984. Geometría y evolución estructural del Manto de Somiedo (Zona Cantábrica, NO de España). Bol. Geol. Min. 95 (6), 3–25.
Beutner, E.C., Diegel, F.A., 1985. Determination of fold kinematics from syntectonic fibers in pressure shadows, Martinsburg slate, New Jersey. Am. J. Sci. 285, 16–50.
Bulnes, M., Poblet, J., Uzkeda, H., Rodríguez-Álvarez, I., 2019. Mechanical stratigraphy influence on fault-related folds development: insights from the Cantabrian zone (NW Iberian Peninsula). J. Struct. Geol. 118, 87–103.
Deere, D.U., Miller, R.P., 1966. Engineering Classification and Index Properties for Intact Rocks. Tech Report Air Force Weapons Lab. AFNL-TR, Kirtland, New Mexico, No, pp. 65–116.
Ferrill, D.A., McGinnis, R.N., Morris, A.P., Smart, K.J., 2012a. Hybrid failure: field evidence and influence on fault refraction. J. Struct. Geol. 42, 140–150.
Ferrill, D.A., McGinnis, R.N., Morris, A.P., Smart, K.J., Sickmann, Z.T., Bentz, M., Lehrmann, D., Evans, M.A., 2014. Control of mechanical stratigraphy on bed-restricted jointing and normal faulting: Eagle Ford Formation, south-central Texas. AAPG (Am. Assoc. Pet. Geol.) Bull. 98 (11), 2477–2506.
Ferrill, D.A., Morris, A.P., McGinnis, R.N., 2012b. Extensional fault-propagation folding in mechanically layered rocks: the case against the frictional drag mechanism. Tectonophysics 576, 78–85.
Ferrill, D.A., Morris, A.P., McGinnis, R.N., Smart, K.J., Ward, W.C., 2011. Fault zone deformation and displacement partitioning in mechanically layered carbonates: the Hidden Valley fault, central Texas. AAPG (Am. Assoc. Pet. Geol.) Bull. 95 (8), 1383–1397.
Ferrill, D.A., Morris, A.P., Wigginton, S.S., Smart, K.J., McGinnis, R.N., Lehrmann, D., 2016. Deciphering thrust fault nucleation and propagation and the importance of footwall synclines. J. Struct. Geol. 85, 1–11.
Greco, R., Sorriso-Valvo, M., 2005. Relationships between joint apparent separation, Schmidt-hammer rebound value, and distance to faults, in rocky outcrops, Calabria, Southern Italy. Eng. Geol. 78 (3–4), 309–320.
Julivert, M., 1971. Décollement tectonics in the Hercynian Cordillera of NW Spain. Am. J. Sci. 270, 1–29.
Julivert, M., 1979. A cross-section through the northern part of the Iberian Massif: its position within the Hercynian fold belt. Krystalinikum 14, 51–67.
Julivert, M., 1981. A cross-section through the northern part of the Iberian Massif: its position within the Hercynian fold belt. Geologie en Minbouw 60, 107–128.
Julivert, M., 1983. La estructura de la Zona Cantábrica. In: Comba, J.A. (Ed.), Geología de España. Libro Jubilar J. M. Ríos, Tomo I. Instituto Geológico y Minero de España, Madrid, pp. 339–381.
Julivert, M., Fontboté, J.M., Ribeiro, A., Conde, L.E., 1972. Mapa Tectónico de la Península Ibérica y Baleares, E. 1:1000000. Instituto Geológico y Minero de España, Madrid.
Katz, O., Reches, Z.E., Baer, G., 2003. Faults and their associated host rock deformation: Part I. Structure of small faults in a quartz–syenite body, southern Israel. J. Struct. Geol. 25 (10), 1675–1689.
Lotze, F., 1945. Zur gliederung der varisziden der Iberischen Meseta. Geotekt. Forsch. 6, 78–92.
Martín, S., Uzkeda, H., Poblet, J., Bulnes, M., 2019. Geological interpretation of two virtual outcrops of deformed Palaeozoic rocks (NW Iberian Peninsula) using 3D Stereo VDT in a computer assisted virtual environment (CAVE™). J. Iber. Geol. 45, 565–584.
Martín, S., Uzkeda, H., Poblet, J., Bulnes, M., Rubio, R., 2013. Construction of accurate geological cross-sections along trenches, cliffs and mountain slopes using photogrammetry. Comput. Geosci. 51, 90–100.
Masini, M., Bulnes, M., Poblet, J., 2010a. Cross-section restoration: a tool to simulate deformation. Application to a fault-propagation fold from the Cantabrian fold and thrust belt, NW Iberian Peninsula. J. Struct. Geol. 32 (2), 172–183.
Masini, M., Poblet, J., Bulnes, M., 2010b. Structural analysis and deformation architecture of a fault-propagation fold in the southern Cantabrian Mountains, NW Iberian Peninsula. Trab. Geol. 30, 55–62.
McGinnis, R.N., Ferrill, D.A., Morris, A.P., Smart, K.J., Lehrmann, D., 2017. Mechanical stratigraphic controls on natural fracture spacing and penetration. J. Struct. Geol. 95, 160–170.
Morris, A.P., Ferrill, D.A., McGinnis, R.N., 2009. Mechanical stratigraphy and faulting in Cretaceous carbonates. AAPG (Am. Assoc. Pet. Geol.) Bull. 93 (11), 1459–1470.
Navarro Vázquez, D., Rodríguez Fernández, R., 1982. Mapa Geológico de España, E. 1: 50.000. Hoja: 101 Villablino (11-07. Instituto Geológico y Minero de España, Madrid.
Pérez-Estaún, A., Bastida, F., 1990. Cantabrian zone: structure. In: Dallmeyer, R.D., Martínez-García, E. (Eds.), Pre-Mesozoic Geology of Iberia. Springer-Verlag, Berlin, pp. 55–69.
Pérez-Estaún, A., Bastida, F., Alonso, J.L., Marquínez, J., Álvarez-Marrón, J., Marcos, A., Pulgar, J.A., 1988. A thin-skinned tectonics model for an arcuate fold and thrust belt: the Cantabrian Zone (Variscan Ibero-Armorican Arc). Tectonics 7, 517–537.
Poblet, J., 2020. Cartographic pattern of terminations of simple, parallel fault-bend folds, fault-propagation folds and detachment folds. J. Struct. Geol. 138, 104135.
Proceq, 2016. Rock Schmidt. Operating Instructions. Proceq S.A., Schwerzenbach.
QGIS.org Association, 2021. QGIS Geographic Information system. http://www.qgis.org.
Salvini, F., Storti, F., 2001. The distribution of deformation in parallel fault-related folds with migrating axial surfaces: comparison between fault-propagation and fault-bend folding. J. Struct. Geol. 23 (1), 25–32.
Savage, H.M., Shackleton, J.R., Cooke, M.L., Riedel, J.J., 2010. Insights into fold growth using fold-related joint patterns and mechanical stratigraphy. J. Struct. Geol. 32 (10), 1466–1475.
Savage, J.F., 1979. The Hercynian orogeny in the Cantabrian mountains, northern Spain. Krystalinikum 14, 91–108.
Savage, J.F., 1981. Geotectonic cross-section through the Cantabrian mountains, northern Spain. Geol. Mijnbouw 81, 3–5.
Shackleton, J.R., Cooke, M.L., Sussman, A.J., 2005. Evidence for temporally changing mechanical stratigraphy and effects on joint-network architecture. Geology 33 (2), 101–104.
Smart, K.J., Ferrill, D.A., Morris, A.P., Bichon, B.J., Riha, D.S., Huyse, L., 2010. Geomechanical modeling of an extensional fault-propagation fold: big brushy Canyon monocline, Sierra del Carmen, Texas. AAPG (Am. Assoc. Pet. Geol.) Bull. 94 (2), 221–240.

Smart, K.J., Ferrill, D.A., Morris, A.P., McGinnis, R.N., 2012. Geomechanical modeling of stress and strain evolution during contractional fault-related folding. Tectonophysics 576, 171–196.
Smart, K.J., Ofoegbu, G.I., Morris, A.P., McGinnis, R.N., Ferrill, D.A., 2014. Geomechanical modeling of hydraulic fracturing: why mechanical stratigraphy, stress state, and pre-existing structure matter. AAPG (Am. Assoc. Pet. Geol.) Bull. 98 (11), 2237–2261.
Stahl, T., Tye, A., 2020. Schmidt hammer and terrestrial laser scanning (TLS) used to detect single-event displacements on the Pleasant Valley fault (Nevada, USA). Earth Surf. Process. Landforms 45 (2), 473–483.
Steer, P., Bigot, A., Cattin, R., Soliva, R., 2011. In-situ characterization of the effective elasticity of a fault zone, and its relationship to fracture spacing. J. Struct. Geol. 33 (11), 1541–1553.
Suppe, J., 1983. Geometry and kinematics of fault-bend folding. Am. J. Sci. 283, 684–721.
Torabi, A., Alaei, B., Ellingsen, T.S.S., 2018. Faults and fractures in basement rocks, their architecture, petrophysical and mechanical properties. J. Struct. Geol. 117, 256–263.
Tye, A., Stahl, T., 2018. Field estimate of paleoseismic slip on a normal fault using the Schmidt hammer and terrestrial LiDAR: methods and application to the Hebgen fault (Montana, USA). Earth Surf. Process. Landforms 43 (11), 2397–2408.
Uzkeda, H., Poblet, J., Bulnes, M., Martín, S., 2018. Effects of inherited structures on inversion tectonics: Examples from the Asturian basin (NW Iberian Peninsula) interpreted in a computer assisted virtual environment (CAVE). Geosphere 14 (4), 1635–1656.
Wagner, R.H., Prins, C.W., Riding, R.E., 1971. Lithostratigraphic units of the lower part of the Carboniferous in northern León, Spain (with a "Note on some goniatite faunas" by CH WAGNER-GENTIS). Trab. Geol. 4, 603–665.
Wu, C., 2013. Towards linear-time incremental structure from motion. In: Proceedings of the 3DV 2013, Seattle, pp. 127–134.
Zahm, C.K., Zahm, L.C., Bellian, J.A., 2010. Integrated fracture prediction using sequence stratigraphy within a carbonate fault damage zone, Texas, USA. J. Struct. Geol. 32 (9), 1363–1374.